Advances in methods to obtain and characterise room temperature magnetic ZnO

I. Lorite,[1] B. Straube,[2,3] H. Ohldag,[4] P. Kumar,[1,a)] M. Villafuerte,[2,3] P. Esquinazi,[1] C. E. Rodríguez Torres,[5] S. Perez de Heluani,[2] V. N. Antonov,[6,7] L. V. Bekenov,[6,7] A. Ernst,[7,8] M. Hoffmann,[7,9] S. K. Nayak,[9] W. A. Adeagbo,[9] G. Fischer,[7] and W. Hergert[9]
[1]*Division of Superconductivity and Magnetism, Institute for Experimental Physics II, Fakultät für Physik und Geowissenschaften, Linnéstraße 5, 04103 Leipzig, Germany*
[2]*Laboratorio de Física del Sólido, Dpto. de Física, Facultad de Ciencias Exactas y Tecnología, Universidad Nacional de Tucumán, Argentina*
[3]*CONICET, Dpto. de Física, Facultad de Ciencias Exactas y Tecnología, Universidad Nacional de Tucumán, Argentina*
[4]*Stanford Synchrotron Radiation Lightsource, Stanford University, Menlo Park, California 94025, USA*
[5]*IFLP-CONICET, CCT-La Plata and Departamento de Física, Universidad Nacional de La Plata, Argentina*
[6]*Institute for Metal Physics, 36 Vernadsky Street, 03142 Kiev, Ukraine*
[7]*Max Planck Institute of Microstructure Physics, Weinberg 2, 06120 Halle, Germany*
[8]*Wilhelm-Ostwald-Institut für Physikalische und Theoretische Chemie, Universitat Leipzig, Linnéstraße 2, 04103 Leipzig, Germany*
[9]*Institut für Physik, Martin Luther University Halle-Wittenberg, Von-Seckendorff-Platz 1, 06120 Halle, Germany*

(Received 23 January 2015; accepted 17 February 2015; published online 27 February 2015)

We report the existence of magnetic order at room temperature in Li-doped ZnO microwires after low energy H^+ implantation. The microwires with diameters between 0.3 and 10 μm were prepared by a carbothermal process. We combine spectroscopy techniques to elucidate the influence of the electronic structure and local environment of Zn, O, and Li and their vacancies on the magnetic response. Ferromagnetism at room temperature is obtained only after implanting H^+ in Li-doped ZnO. The overall results indicate that low-energy proton implantation is an effective method to produce the necessary amount of stable Zn vacancies near the Li ions to trigger the magnetic order. © *2015 AIP Publishing LLC*. [http://dx.doi.org/10.1063/1.4913763]

During the last fifteen years, many articles reported that certain semiconductors become magnetically ordered at room temperature (RT) upon doping with magnetic ions.[1–6] However, there is now consent that the origin of the magnetically ordered state in diluted oxide semiconductors is related to lattice defects and/or added ions, which are not necessarily magnetic, a phenomenon called defect-induced magnetism.[7–13] Nevertheless, in spite of the large number of experimental studies, there is no simple method to introduce systematically the required defect concentration in the corresponding lattice sites. Moreover, low resistivity and magnetic *p*-type oxides, necessary for further implementation in electronic devices, remain an unresolved goal partially because of the formation of oppositely charged defects, which pin the Fermi level.[14] The most likely cause for the doping difficulty is the formation of interstitials of group-I elements and antisites of group-V elements.[15–17]

A method to produce *p*-type ZnO by co-doping ZnO with H and Li or Na has been proposed.[18] In this case, the introduction of H suppresses severely the formation of compensating interstitials, enhancing the acceptor solubility by forming H-acceptor complexes. In this article, we show that by implanting H^+ at low energies into Li-doped ZnO we solve two experimental problems simultaneously. From one side, the low energy implantation produces Zn vacancies (V_{Zn}) with a concentration of the order of the doped Li concentration without disturbing too much the ZnO lattice. Simultaneously, the implanted H^+ generates the necessary defect-complexes that stabilise the concentration of V_{Zn}.

The necessary magnetic characterisation has been carried out combining X-ray magnetic circular dichroism (XMCD) and SQUID magnetisation measurements. Spectroscopic methods (Raman and photoluminescence (PL)) have been used to elucidate the relationship between the doping, the produced defects, and the magnetic order. Pure and Li-doped ZnO powders were obtained by thermal decomposition of zinc acetate ($Zn(Ac)_2$). As starting precursors $Zn(Ac)_2$ dihydrate $Zn(CH_3COO)_2 \cdot 2H_2O$ and Li-hydroxide mono hydrate $LiOH \cdot H_2O$ of (Sigma-Aldrich) (99.99%) commercial chemicals were used. The precursors were mixed in 30 ml of tri-distilled water at a nominal concentration of 1, 3, and 7 at. % Li/Zn. After dehydration, the mixture was placed in an oven for different annealing steps. During the thermal treatment, the sample was kept at a partial vapour pressure of 18 kPa of water. Afterwards, the obtained powders were milled and sintered at 900 °C during 1 h in order to grow ZnO microwires (MWs) by a carbothermal process using the procedure described in Ref. 19. The obtained wires, i.e., pure ZnO and Li-doped ZL1, ZL3, and ZL7 (1, 3, 7% Li nominal concentration, respectively) showed wurzite like structure with hexagonal morphology with the c-axis as main wire growth axis. The MW grew showing a wide range of diameters between a few hundreds

[a)]On leave from Department of Physics, Indian Institute of Technology Delhi, New Delhi - 110016, India

 © 2015 AIP Publishing LLC

TH-2015-05
This article is copyrighted as indicated in the article. Reuse of AIP content is subject to the terms at: http://scitation.aip.org/termsconditions. Downloaded to IP: 192.108.69.16 On: Sun, 01 Mar 2015 09:34:58

of nm up to 10 μm and a maximum length of 3 mm. The pure and the Li-doped MW were exposed to remote hydrogen DC plasma (300 eV H^+ implantation energy) in the parallel-plate configuration using a procedure described in Ref. 20. There is a qualitative correlation between the different lithium concentrations in source powders with Raman and PL spectroscopic signals from the microwires, compatible with the physics described below.

Figure 1 shows the Raman spectra of the different Li doped ZnO MW before H^+ implantation at RT. Notice that for these three samples, the modes E2(High) and E1(LO), related to oxygen, show similar intensity suggesting that Li doping does not have a relevant influence on the oxygen vacancies production. On the other hand, there is a clear reduction of the Zn-sublattice related modes, i.e., A1(TO), E1(TO), and E2(High)-E2(Low) peaks increasing Li concentration, suggesting that the Zn stoichiometry changes, consistent with X-ray Absorption Spectroscopy (XAS) results shown below.

Photoluminescence spectra at 300 K have been measured for all samples before H^+ implantation. As example, in the inset of Fig. 1, we show the PL spectrum for sample ZL3. It shows the well known defect band and the UV emission band between 3.20 and 3.40 eV, where two different peaks can be resolved at 3.294 eV and at 3.211 eV due to free electron-acceptor and donor-acceptor recombinations.[21] From this spectrum, we obtain the binding energy of Li acceptors, $E_{\mathrm{Li_A}} \simeq 0.142$ eV, which agrees with the reported binding energy of the shallow acceptor (0.150 eV) in Li-doped ZnO.[21]

The magnetic properties of the different samples were investigated at RT, before and after H^+ implantation measuring the magnetisation. Figure 2 shows the hysteresis loops of ZL1, ZL3, and ZL7 samples after subtracting the diamagnetic contribution of the substrates used to hold the wires. A magnetic moment $m < 2 \times 10^{-7}$ emu was measured for ZL1 (see Fig. 2(a)). This moment did not change after H^+ implantation and it remained within the range of SQUID resolution, corroborating the non-magnetic behavior of ZL1.

The hysteresis loops for ZL3 and ZL7 samples, Figures 2(b) and 2(c), confirm the ferromagnetic behaviour for these

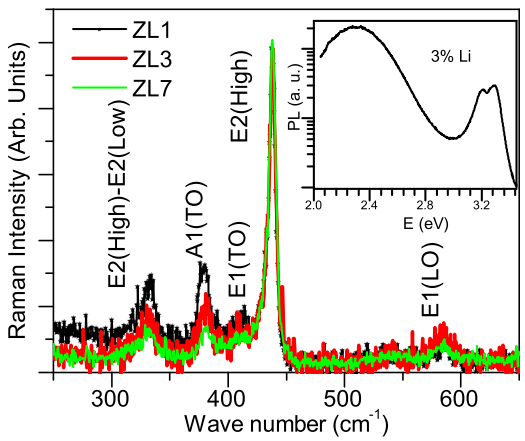

FIG. 1. Raman spectroscopy at room temperature of the different Li doped ZnO MW. The inset shows the PL spectrum for sample ZL3 before implantation.

Li contents but only after H^+ implantation. Note that the maxima of the saturation magnetisation increase with H^+ implantation time. Around 90 min was the time at which the magnetic signal reached the maximum saturation value; further implantation time did not result in a larger magnetic moment. This indicates that there is a concentration of H^+ at which it is possible to obtain the maximum of saturation magnetisation. During 1 h at a H^+ current of 60 μA on the exposed surface of the conglomerate of $\sim$0.1 cm^2 area fixed on a conducting substrate of $\simeq$0.5 cm^2, one implants the amount of $\sim 3 \times 10^{18}$ H^+/cm^2 in the first $\simeq$10 nm at an energy of 300 eV according to SRIM simulations,[22] used also to estimate the density of Zn and O vacancies produced by the implantation of the low energy H^+. Assuming a displacement energy of 18.5 eV for Zn in a pure ZnO lattice[23] the SRIM estimate gives $\sim(3 \pm 2) \times 10^{22}$ V_{Zn}/cm^3 in the first 10 nm (the error is the maximum uncertainty due to geometrical factors). This V_{Zn} concentration is $\sim$10 times larger than the Li concentration $\sim 3 \times 10^{21}$ cm^{-3} assuming the nominal concentration of 7%. We note, however, that SRIM does not take into account the diffusion and annihilation of point defects due to the temperature. These processes decrease substantially the amount of V_{Zn} in the ZnO lattice. Taking a penetration depth of 10 nm, we estimate a maximum number of Li atoms of $\sim 3\ (1.3) \times 10^{14}$ for the ZL7 (ZL3) sample. *Ab initio* calculations explained below provide magnetic moment values for the Li-V_{Zn} with H^+ between 1 and $\sim 2\ \mu_B$.

To further investigate the nature of the magnetic order in the MW, XMCD measurements were carried out at the soft x-ray elliptical undulator beamline 13-1 at the Stanford Synchrotron Radiation Lightsource. XMCD allows to separate the contributions to the macroscopic magnetic moment in an element specific way by tuning the energy of the incoming x-rays to the absorption resonance of the atomic species of interest. For this XMCD study, we focused on two particular samples, i.e., the non-magnetic, ZL1, and one magnetic, ZL3. XAS were taken at two different edges, i.e., the Zn L-edge and O K-edge with circular polarization, see Fig. 3. The experimental XAS result in Fig. 3(d) is in good agreement with a recently published one.[24] The XMCD difference was obtained by subtracting two spectra that were acquired sequentially with alternating magnetic fields of ± 2 kOe. In Fig. 3(a), we show that there is no evidence of XMCD for ZL1 at both edges, in agreement with the SQUID results. However, there is a clear XMCD signal for ZL3 in the range of 533–540 eV, which corresponds to the polarization of the O K-edge, see Fig. 3(d), whereas no magnetic signal is found for the Zn L-edge in Fig. 3(c). This in agreement with our calculations shown below, and as well as previous results,[25] showing that the density of states of the O-2*p* band from oxygen atoms around a V_{Zn} is polarised.

To elucidate the experimental finding, we performed extensive first-principles calculations. Since the crystalline structure and the amounts of the different defective or pure phases of the probed samples are not exactly known, we modelled various configurations of H^+-implanted Li-doped ZnO with Zn and O vacancies and calculated XAS and XMCD spectra. Since the defective region is localised in only a small part of the sample, it is expected that the

This article is copyrighted as indicated in the article. Reuse of AIP content is subject to the terms at: http://scitation.aip.org/termsconditions. Downloaded to IP: 192.108.69.16 On: Sun, 01 Mar 2015 09:34:58

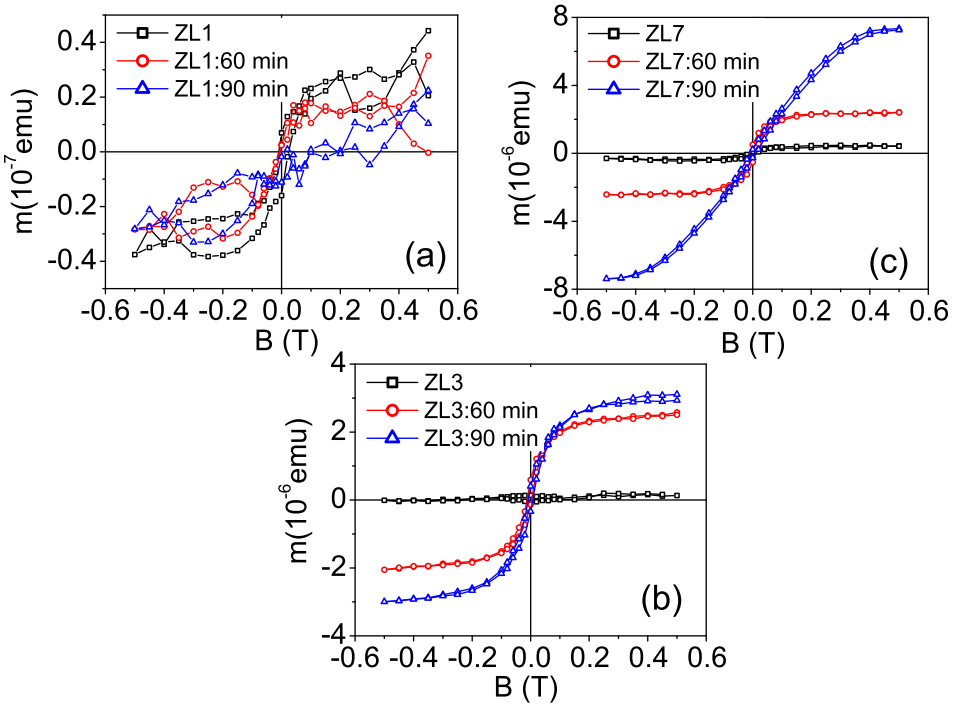

FIG. 2. Magnetic field hysteresis loops of the magnetic moment for: (a) ZL1, (b) ZL3, and (c) ZL7 samples, after subtracting the diamagnetic background and after different and consecutive H^+ treatments.

experimental result represents a mixture of different contributions. This enables us to elucidate the real structure and chemical composition of a sample by comparing the theoretical and the experimental XAS and XMCD spectra.

The details of the computational method are described in our previous papers,[26–28] and here, we only mention some aspects specific to the present calculations. The XAS and XMCD simulations were performed using the spin-polarised fully relativistic linear-muffin-tin-orbital (SPR LMTO) method,[29,30] while the structures were obtained with a projector-augmented wave pseudo-potential method[31] including Hubbard corrections[32] implemented in the VASP code,[33–35] which is well known for precise total energy and forces calculations. In our study, we tried several configurations placing H^+ and Li-, Zn- and O-vacancies in various positions, and in various combinations examining the electronic and magnetic structures. From the systems containing V_{Zn}, only those in which the V_{Zn} are placed far away from H and Li were magnetic as well. Our results indicate that the Li atoms act as *p* dopant increasing the number of holes, and the irradiated protons are responsible for creating V_{Zn}, but neither H nor Li participate directly in the magnetic moment formation. Oxygen vacancies not only do not contribute to magnetic moment formation but also they annihilate any *p*-hole moments due to their donor-like character.[36]

The comparison between the experimental and the calculated results is given in Fig. 4. We present three theoretical cases: (i) perfect ZnO, (ii) ZnO with a Zn vacancy, and (iii) ZnO with a Zn vacancy and Li co-doping. The experimental XAS spectrum can be explained by a combination of these

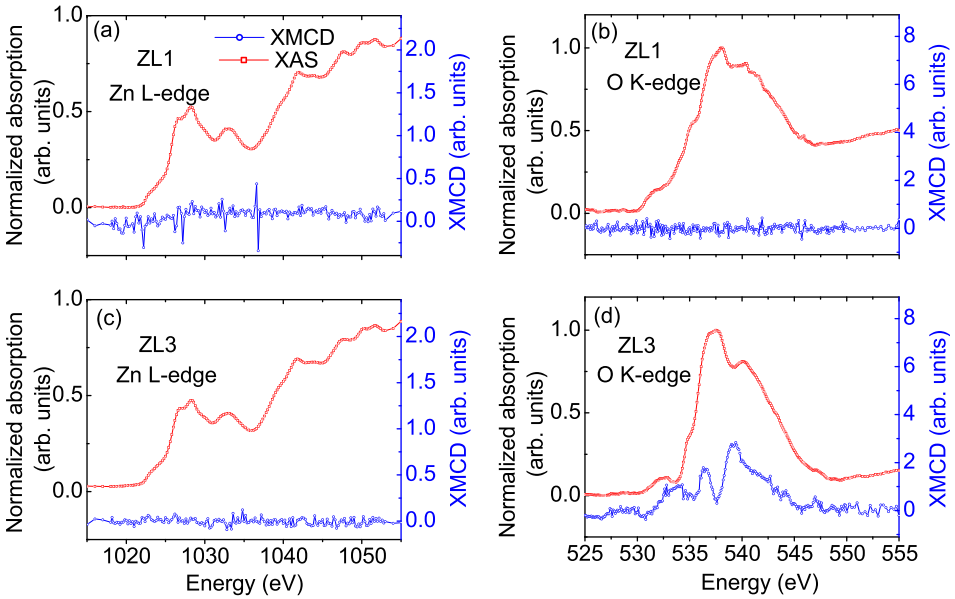

FIG. 3. XAS and XMCD at the Zn L-edge and O K-edge for the non-magnetic ZL1 and magnetic ZL3 samples after H^+ implantation.

This article is copyrighted as indicated in the article. Reuse of AIP content is subject to the terms at: http://scitation.aip.org/termsconditions. Downloaded to IP: 192.108.69.16 On: Sun, 01 Mar 2015 09:34:58

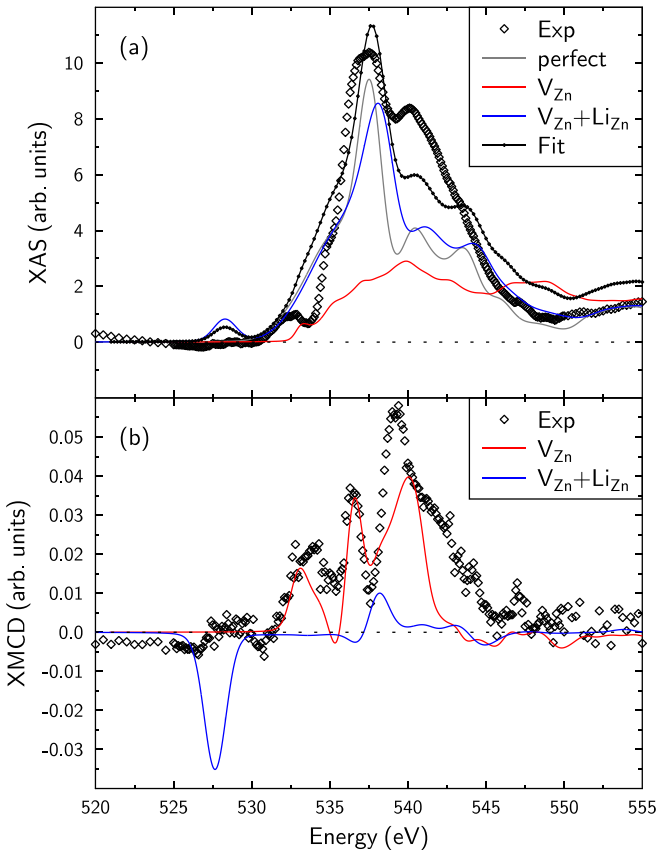

FIG. 4. Experimental (sample ZL3 after H^+ implantation) and theoretical XAS (a) and XMCD (b)at the O K-edge for perfect ZnO, ZnO with Zn vacancies (5.56% V_{Zn} concentration), and with Zn vacancy near a Li ion substituting Zn. The XAS fit (black curve) is calculated adding the different weighted contributions.

theoretical models, where the case of Li does not seem necessary at first sight. In particular, the peak slightly below 528 eV cannot be found in the experiment, which points to few Li atoms in the detectable sample region. Generally, the experimental XAS signal is weighted mainly by perfect ZnO, as the simulations indicate, see Fig. 4.

In contrast, the experimental XMCD spectra in Fig. 4(b) are well explained by the simulated V_{Zn} case. Moreover, the experimental features around 528 eV can possibly be explained by a small contribution of $V_{Zn} + Li_{Zn}$ spectrum. We can, therefore, conclude that in the real samples the significant part of the XMCD signal comes from the Zn vacancy case without Li co-doping, while the XAS spectra are dominated by the perfect ZnO. This indicates the separation of different magnetic and non-magnetic phases in real samples, possibly due to spinodal decomposition.[37] The absolute values of the saturation magnetic moments, see Fig. 2, indicate therefore that the magnetic order comes from a V_{Zn} with magnetic moment $m \sim 2\,\mu_B$,[36,38] and a concentration of the order of the Li concentration, supporting the argument that the presence of Li stabilises the produced V_{Zn}.[18] The spin-polarisation due to the unsaturated O-2*p* bonds is related to the creation of a hole.

In conclusion, we report evidence of magnetic order at ambient conditions due to the O-2*p* spin polarization induced by the proximity to zinc vacancies. The zinc vacancies are stabilized by Li doping and produced by H^+ implantation at low energies, a method that combined with Li-doping opens up a reproducible way to obtain high-temperature magnetic order in ZnO, and possibly also in other non-magnetic oxides semiconductors.

This work was funded by Secyt-UNCor, CIUNT and Conicet in Argentina, the Collaborative Research Center SFB 762 "Functionality of Oxide Interfaces" in Germany and DAAD-PROLAR Project 57052290. Use of the Stanford Synchrotron Radiation Lightsource, SLAC National Accelerator Laboratory, is supported by the U.S. Department of Energy, Office of Science, and Office of Basic Energy Sciences under Contract No. DE-AC02-76SF00515.

[1]T. Dietl, H. Ohno, F. Matsukura, J. Cibert, and D. Ferand, Science **287**, 1019 (2000).
[2]J. M. D. Coey, M. Venkatesan, and C. B. Fitzgerald, Nat. Mater. **4**, 173 (2005).
[3]K. Ueda, H. Tabata, and T. Kawai, Appl. Phys. Lett. **79**, 988 (2001).
[4]F. Golmar, M. Villafuerte, A. Mudarra Navarro, C. Rodríguez Torres, J. Barzola-Quiquia, P. Esquinazi, and S. Heluani, J. Mater. Sci. **45**, 6174 (2010).
[5]K. Sato, W. Schweika, P. H. Dederichs, and H. Katayama-Yoshida, Phys. Rev. B **70**, 201202 (2004).
[6]K. Sato, L. Bergqvist, J. Kudrnovský, P. H. Dederichs, O. Eriksson, I. Turek, B. Sanyal, G. Bouzerar, H. Katayama-Yoshida, V. A. Dinh *et al.*, Rev. Mod. Phys. **82**, 1633 (2010).
[7]H. Peng, H. J. Xiang, S.-H. Wei, S.-S. Li, J.-B. Xia, and J. Li, Phys. Rev. Lett. **102**, 017201 (2009).
[8]M. D. McCluskey and S. J. Jokela, J. Appl. Phys. **106**, 071101 (2009).
[9]G. Z. Xing, Y. H. Lu, Y. F. Tian, J. B. Yi, C. C. Lim, Y. F. Li, G. P. Li, D. D. Wang, B. Yao, J. Ding *et al.*, AIP Adv. **1**, 022152 (2011).
[10]P. Esquinazi, W. Hergert, D. Spemann, A. Setzer, and A. Ernst, IEEE Trans. Magn. **49**, 4668 (2013).
[11]C. Guglieri, E. Céspedes, A. Espinosa, M. N. Laguna-Marco, N. Carmona, Y. Takeda, T. Okane, T. Nakamura, M. García-Hernández, M. N. García *et al.*, Adv. Funct. Mater. **24**, 2094 (2014).
[12]K. Kenmochi, V. A. Dinh, K. Sato, A. Yanase, and H. Katayama-Yoshida, J. Phys. Soc. Jpn. **73**, 2952 (2004).
[13]H. Katayama-Yoshida, K. Sato, T. Fukushima, M. Toyoda, H. Kizaki, V. A. Dinh, and P. H. Dederichs, Phys. Status Solidi A **204**, 15 (2007).
[14]V. Avrutin, D. Silversmith, and H. Morkoc, Proc. IEEE **98**, 1269 (2010).
[15]A. Zunger, Appl. Phys. Lett. **83**, 57 (2003).
[16]C. H. Park, S. B. Zhang, and S.-H. Wei, Phys. Rev. B **66**, 073202 (2002).
[17]R.-Y. Tian and Y.-J. Zhao, J. Appl. Phys. **106**, 043707 (2009).
[18]L. Eun-Cheol and K. J. Chang, Phys. Rev. B **70**, 115210 (2004).
[19]M. Villafuerte, J. M. Ferreyra, C. Zapata, J. Barzola-Quiquia, F. Iikawa, P. Esquinazi, S. P. Heluani, M. M. de Lima, and A. Cantarero, J. Appl. Phys. **115**, 133101 (2014).
[20]I. Lorite, P. Esquinazi, C. Zapata, and S. P. Heluani, J. Mater. Res. **29**, 78 (2014).
[21]C. Rauch, W. Gehlhoff, M. R. Wagner, E. Malguth, G. Callsen, R. Kirste, B. Salameh, A. Hoffmann, S. Polarz, Y. Aksu *et al.*, J. Appl. Phys. **107**, 024311 (2010).
[22]J. F. Ziegler, J. P. Biersack, and M. D. Ziegler, *SRIM - The Stopping and Range of Ions in Matter* (SRIM Co., 2008); see http://www.ele.uva.es/jesman/iis.html for some advantages in comparison with the usual SRIM simulation.
[23]H. Tsuchihira, T. Oda, and S. Tanaka, Nucl. Instrum. Methods Phys. Res., Sect. B **269**, 1707 (2011).
[24]S. B. Singh, Y.-F. Wang, Y.-C. Shao, H.-Y. Lai, S.-H. Hsieh, M. V. Limaye, C.-H. Chuang, H.-C. Hsueh, H. Wang, J.-W. Chiou *et al.*, Nanoscale **6**, 9166 (2014).
[25]J. B. Yi, C. C. Lim, G. Z. Xing, H. M. Fan, L. H. Van, S. L. Huang, K. S. Yang, X. L. Huang, X. B. Qin, B. Y. Wang *et al.*, Phys. Rev. Lett. **104**, 137201 (2010).
[26]V. N. Antonov, H. A. Dürr, Y. Kucherenko, L. V. Bekenov, and A. N. Yaresko, Phys. Rev. B **72**, 054441 (2005).
[27]V. N. Antonov, O. Jepsen, A. N. Yaresko, and A. P. Shpak, J. Appl. Phys. **100**, 043711 (2006).
[28]V. N. Antonov, A. N. Yaresko, and O. Jepsen, Phys. Rev. B **81**, 075209 (2010).

This article is copyrighted as indicated in the article. Reuse of AIP content is subject to the terms at: http://scitation.aip.org/termsconditions. Downloaded to IP: 192.108.69.16 On: Sun, 01 Mar 2015 09:34:58

[29]O. K. Andersen, Phys. Rev. B **12**, 3060 (1975).
[30]V. V. Nemoshkalenko, A. E. Krasovskii, V. N. Antonov, V. N. Antonov, U. Fleck, H. Wonn, and P. Ziesche, Phys. Status Solidi B **120**, 283 (1983).
[31]P. E. Blöchl, Phys. Rev. B **50**, 17953 (1994).
[32]V. I. Anisimov, J. Zaanen, and O. K. Andersen, Phys. Rev. B **44**, 943 (1991).
[33]G. Kresse and J. Hafner, Phys. Rev. B **49**, 14251 (1994).
[34]G. Kresse and J. Furthmüller, Comput. Mater. Sci. **6**, 15 (1996).
[35]J. Hafner, J. Comput. Chem. **29**, 2044 (2008).
[36]W. A. Adeagbo, G. Fischer, A. Ernst, and W. Hergert, J. Phys.: Condens. Matter **22**, 436002 (2010).
[37]K. Sato, H. Katayama-Yoshida, and P. H. Dederichs, Jpn. J. Appl. Phys., Part 2 **44**, L948 (2005).
[38]T. Chanier, I. Opahle, M. Sargolzaei, R. Hayn, and M. Lannoo, Phys. Rev. Lett. **100**, 026405 (2008).

This article is copyrighted as indicated in the article. Reuse of AIP content is subject to the terms at: http://scitation.aip.org/termsconditions. Downloaded to IP: 192.108.69.16 On: Sun, 01 Mar 2015 09:34:58